Enhanced mixing in laminar flows using ultrahydrophobic surfaces

Jia Ou, Geoffrey R. Moss, and Jonathan P. Rothstein
Department of Mechanical and Industrial Engineering, University of Massachusetts, Amherst, Massachusetts 01003-2210, USA
(Received 5 March 2007; published 12 July 2007)

Under laminar, microscale flow conditions, rapid mixing can be difficult to achieve. In these low Reynolds number flows, mixing rates are governed by molecular diffusion, and in the absence of enhanced mixing techniques, mixing lengths and residence times can be much longer than most applications will allow. A number of active mixing techniques have been developed to improve mixing; however, they can be complex to implement and expensive to fabricate. In this paper, we describe a passive mixing method that utilizes a series of ultrahydrophobic surfaces. Our previous experiments have demonstrated that a shear-free air-water interface supported between hydrophobic microridges results in large slip velocities along these ultrahydrophobic surfaces, and significant drag reduction. By aligning the microridges and therefore the air-water interface at an oblique angle to the flow direction, a secondary flow is generated, which is shown to efficiently stretch and fold the fluid elements and reduce the mixing length by more than an order of magnitude compared to that of a smooth microchannel. The designs of the ultrahydrophobic surfaces were optimized through experiments and numerical simulations. A Y-shaped channel was used to bring two streams of water together, one tagged with a fluorescent dye. A confocal microscope was used to measure fluorescence intensity and dye concentration. Quantitative agreement between the experiments and the numerical simulations was achieved for both the flow patterns and degree of mixing. Increasing the angle of the microridges was found to reduce the mixing length up to a critical angle of about 60°, beyond which the mixing length was found to increase with further increases to the angle of the microridge. The mixing enhancement was found to be much less sensitive to changes in microridge width or separation.

DOI: 10.1103/PhysRevE.76.016304 PACS number(s): 47.61.Ne

I. INTRODUCTION

Rapid fluid mixing is essential to many microfluidic systems used in such scientifically and economically important fields as biochemical analysis, drug delivery, and microassaying on chips [1,2]. Molecular diffusion may be sufficient to mix ultrasmall volumes of fluid in the subpicoliter range. However, in the absence of turbulent convection, mixing of larger volumes of fluids in microchannels at low Reynolds numbers is difficult, and often requires resourceful combinations of both convection and diffusion to reduce processing times, path lengths, and pressure drops to within acceptable levels [2–8]. Developing techniques to enhance mixing, specifically passive mixing, in microchannels beyond molecular diffusion limits [9] is therefore of extreme commercial and scientific importance. Several schemes for passive mixing have been developed and studied, including T-type mixers [10], serpentine channels [5], and flow splitting [11]. Because mixing at low Reynolds number is controlled by molecular diffusion, inducing the growth of vortices or flow patterns which stretch and fold fluid elements can bring the two fluids to be mixed closer together, thereby significantly reducing the time and the length of channel required to adequately mix the fluid components [12]. Furthermore, the motion of fluid particles can be made chaotic by eliminating the integrability of the advection equations and making a steady microflow suitably three dimensional or time dependent [5,12]. In this paper, we will demonstrate through both detailed experiments and numerical simulations that enhanced mixing in laminar flows in microchannels can be achieved using ultrahydrophobic surfaces containing microridges aligned obliquely to the flow direction.

Ultrahydrophobic or superhydrophobic surfaces were originally inspired by the unique water-repellent properties of the lotus leaf [13]. Recent synthetic surfaces have been developed that are capable of obtaining contact angles that can approach $\theta=180°$ [14–19]. Ultrahydrophobic surfaces are rough with micrometer-sized protrusions coming out of the surface. In the Wenzel state [20], the water penetrates into the corrugations on the surface. However, in the Casie state [21], the hydrophobicity of the microscale surface roughness prevents the water from moving into the space between the peaks of the surface roughness, resulting in an air-water interface as seen schematically in Fig. 1. The result is the near elimination of the contact angle hysteresis, and a dramatic reduction of the resistance to drop motion [15,18,22]. Additionally, for flows in microchannels, ultrahy-

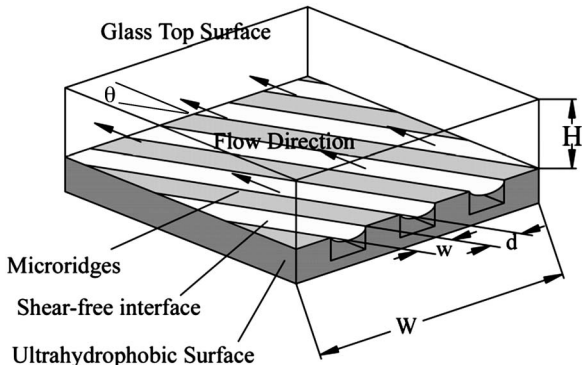

FIG. 1. Schematic diagram of a model for ultrahydrophobic drag reduction. A combination of surface hydrophobicity and roughness allows water to stand away from the solid surface.

drophobic surfaces have been shown to produce drag reduction even in the absence of contact lines [23–25].

Using lithographically etched silanized silicon surfaces with precisely controlled microsurface topology consisting of regular arrays of microposts and microridges aligned in the flow direction, Ou *et al.* [23,24] systematically investigated the effect of topological changes on drag reduction and velocity profiles, using pressure drop measurements and microparticle image velocimetry (μPIV). At the microchannel length scales investigated in their experiments, the boundary condition for the fluid in contact with the top of the micropost or microridge is no slip; however, the air-water interfaces supported between microposts or microridges are shear-free, essentially providing no resistance to the flow. Ou *et al.* [23] demonstrated the existence and subsequent deflection of the air-water interface under flow, through laser confocal surface metrology measurements of the interface. Pressure drop reductions in excess of $\Pi=(\Delta p_{\text{no slip}}-\Delta p)/\Delta p_{\text{no slip}}>35\%$, slip lengths greater than $b>20$ μm, and slip velocities of more than 50% the average velocity in the microchannel were achieved through a reduction of the effective surface area of the solid in contact with the flowing fluid [23,24]. Additionally, because the surface topology of the photolithographically etched silicon surface could be precisely designed and controlled, Ou *et al.* [23,24] were able to compare the results of their drag reduction measurements directly to analytical solutions and the predictions of numerical simulations.

A host of active mixing techniques have been proposed to enhance mixing in laminar flows. In active mixing, energy is introduced into the microfluidic device through the use of a magnetic field, an electric field, a thermodynamic medium, variable pumping, or a combination of some or all of these effects [26–28]. Recently, it has been shown that significantly enhanced mixing could be achieved in thermocapillary free-surface flow across microstripes when a temperature gradient (induced surface tension gradient) is imposed at a 45° angle to the flow direction. These temperature gradients induced a helical flow pattern that significantly increased mixing [27]. Similar results have also been achieved by applying electric fields and pressure gradients transverse to the flow direction [26].

Ajdari [26] developed a model under the framework of linear-response theory for quantifying the off-diagonal possible in pressure- and electro-osmotically driven flow through microchannels. In this work, Ajdari demonstrated that periodic modulation of the shape of the channel or the surface charge density could result in electro-osmotic flow transverse to the primary flow direction, resulting in enhanced mixing. Ajdari's analysis was later expanded by Stroock *et al.* [29] to look at the specific case of the mixing achieved in pressure-driven flows across surfaces with periodic grooves aligned at an oblique angle to the flow direction.

Niu and Lee [1] investigated microchannel mixing generated by transverse pressure pulses. Two species of fluid were driven by periodic pressure pulses through a main channel that has several pairs of side channels opening into a long main channel. The perturbations were applied transversally to the main flow, resulting in a reduction in the mixing lengths by as much as 10^5. A mixing channel with one pair of side channels was realized by Lee *et al.* [30]. The pressure of the side channel was controlled by high-speed solenoid valves, and lobelike distortions of the interface were observed to facilitate the rapid mixing. These active mixing methods are capable of precisely controlling the flow to generate the chaotic motion needed to produce the desired mixing enhancement. Unfortunately, the fabrication and operation of these microfluidic devices can be rather complicated and expensive.

Alternatively, a number of passive mixing approaches have also been proposed. Passive mixing techniques are very popular, and widely used in both research and industry. The degree of passive mixing can be controlled by the design of the microchannel [5,12,31] or the surface patterns on the channel walls [2,32,33]. With little environmental requirements and no need for elaborate pumps or valves, these passive techniques are promising for applications of microfluidics in chemical engineering and biotechnology, such as lab-on-chip technology and biological and medical analysis.

In passive mixing schemes, the microchannel's geometry is often designed for three-dimensional (3D) flow, which can stretch and fold the fluid elements to be mixed. For example, a three-dimensional serpentine microchannel was designed by Liu *et al.* [5] using photolithographic etching from both sides of a silicon substrate. Even at very low Reynolds numbers, the 3D serpentine channel was found to enhance the rate of mixing to more than 16 times that of a straight channel, and to 1.6 times that of a 2D serpentine channel. Simonnet and Groisman [31] successfully enhanced mixing using a channel with a series of repeating stirring segments designed to generate a three-dimensional chaotic flow. Still other research focused on the geometry of the channel's inner surface.

In the experiments of Johnson *et al.* [32] and Stroock *et al.* [2,29], a series of microridges were fabricated on the bottom of a polydimethylsiloxane (PDMS) microchannel at an oblique angle to the flow direction. A number of different microridge patterns were tested. The simplest pattern incorporated microridges of various depths, widths, and spacings aligned at a 45° angle from the flow direction [2,29]. Using a Y-shaped junction, fluorescently tagged fluids were used to partially fill the mixing channel, and the flow was driven by a pressure drop at Reynolds numbers less than $\mathrm{Re}=UL/\nu<100$ and Péclet numbers greater than $\mathrm{Pe}=UL/D>2000$. Here, U is the average velocity in the channel, L is a cross-sectional dimension like the hydraulic diameter, ν is the viscosity, and D is the self-diffusion coefficient. The mixing was quantified by taking the standard deviation of the intensity distribution of the confocal images of the channel cross section. In the mixing channel, there was less resistance to the flow in the direction parallel to the peaks and the valleys of the microridges than in the orthogonal direction. As a result of this anisotropy, an axial pressure gradient along the microridges generated a transverse velocity tangent to the surface structure at the bottom of the mixing channel, resulting in a helical secondary flow. The fluid then circulated back across the channel along the top wall. Optical images showed the helical secondary flow pattern in the channel and the resulting mixing length reduction.

Stroock *et al.*'s studies showed that increasing the depth or frequency of microridges increased the strength of the helical flow and the rate of mixing. Additionally, Stroock *et al.* [2] demonstrated that mixing could be significantly improved if the design of the microridges was modified to a herringbone pattern in order to generate chaotic flow.

In order to maximize the strength of the secondary flow generated by the surface patterning of the type used by Johnson *et al.* and Stroock *et al.* [2,29,32], Stroock *et al.* [29] demonstrated that one needs to maximize the difference between the drags perpendicular to and parallel to the direction of the microridge. In this paper, we will demonstrate that, due to the presence of a shear-free air-water interface supported between the structures along an ultrahydrophobic surface, this drag differential and in turn the benefits of enhanced mixing can be maximized significantly, outperforming the fully wetted micropatterned surfaces with the added benefit of reducing the drag in the microchannel. In addition, the micromixing flow cell with ultrahydrophobic surfaces has a broader impact on lab-on-chip applications, because it grants access within a closed system to a vapor-liquid interface. Without penetrating between the surface structures, the fluid in the microchannel has a stable interface with the vapor trapped within the surface structures. This interface can be utilized for controlled diffusion from the vapor phase into the liquid phase and provides an ideal channel reaction platform, where the speed of mixing and reaction can be reliably controlled.

The outline of the paper is as follows. In Sec. II we will talk about the experimental setup, fabrication techniques, and numerical simulation. In Sec. III, the experimental results will be analyzed and compared with simulations. Finally, in Sec. IV we conclude.

II. EXPERIMENT

A. Fabrication of the mixing flow channel

The microchannels used in these experiments were fabricated from polydimethylsiloxane (Sylgard 170, Dow Corning) using the soft lithography technique [2]. A master consisting of the negative of a Y-shaped channel 100 μm wide and 50 μm deep was etched on a smooth silicon wafer, using standard photolithography techniques [23,24]. A second photolithographic etching process was used to transfer a series of microridges to the stem of the Y-shaped channel. The microridges were 5 μm deep with width of 30 mm and spacings between microridges in the range $30<d<90$ μm at angles $30°<\theta<90°$ from the flow direction. The wafers were then made hydrophobic through a vapor reaction with dimethylchlorosilane (heptadecafluoro-1,1,2,2-tetrahydrodecyldimethylchlorosilane, Gelest Inc., PA) for 72 h at 65 °C to ensure easy mold release. The PDMS was mixed and applied to the silicon master wafer and then heated with a hotplate for 10 min at 100 °C to be cured. The same vapor reaction that was used to silanize the silicon wafer master was then used to make the microchannel and microridges hydrophobic. During the final vapor reaction, only the areas along the PDMS surface that would be found within the microchannel, and including the microridges, were silanized. The rest of the PDMS surface was masked off and protected from silanization to ensure that these areas would bind to a glass cover slip and form a well-sealed microfluidic device. The cast PDMS channel was bonded to a 22×40 mm^2 microscope cover glass (No. 0, Esco, Erie Scientific Co.) for optical study by plasma etching the cover glass with a plasma cleaner (PDC-001, Harrick Scientific Corp.) for 5 min before it was pressed to the PDMS surface containing the microchannel pattern. The mixing flow cell was completed by attaching a back plate along with inlet and outlet tubes.

B. Flow pattern observation with confocal microscope

A number of techniques exist for observing flow behavior in microfluidic devices [2,24,34,35]. In our previous work, an epifluorescent microscope was used to make μPIV measurements by tracking the motion of fluorescently tagged nanometer-sized seed particles. However, in the mixing experiments described below, the flow is three dimensional, making μPIV measurements and determination of out-of-plane motion difficult. In the measurements described below, confocal microscopy was utilized to measure the relative concentration of a fluorescent dye at several locations along the channel, and to map out the three-dimensional flow patterns induced by the flow across these ultrahydrophobic surfaces and quantify the degree of mixing. The confocal system has two pinholes, one in front of the light source and a second pinhole in front of the detector that ensures that only the image at the focal point of the objective can pass through the pinhole and be captured by the detector. The disadvantage of a confocal microscope is that it is relatively slow, because one must build up an image one pixel at a time; however, in these experiments, confocal microscopes have a distinct advantage over conventional microscopes in that the depth of field is dramatically reduced. The results from a confocal measurement are a stack of images of the fluorescence concentration in the xy plane at depth increments of $\Delta z=0.1$ μm across the channel. The stacks are then assembled into a three-dimensional images using image processing software (IMAGE-J), and resliced into a stack of fluorescent concentration images in the xz plane.

C. Microparticle image velocimetry

To study the flow behavior inside the mixing channel, the detailed slip velocity profile near the ultrahydrophobic surfaces was measured using microparticle image velocimetry (μPIV). In the experiments, an epifluorescent microscope (Nikon TE2000-U) was used to observe the same mixing channels used in confocal observations. The distilled deionized water coming in from one of the inlets was seeded with fluorescently tagged Nile red aliphatic latex spheres 1 μm in diameter (6-NF-1000, Interfacial Dynamics Corp.). The fluorescent particles were chosen to absorb the green incident light and emit red light. For the purpose of capturing the velocity profile near the ultrahydrophobic surface, the particles can be evenly distributed along the top of the surface structures by adjusting the different flow rates of the two inlets. The flow rate of the unseeded fluid in the μPIV ex-

periments is set nine times higher than that of the seeded fluid (1 μl/min), making it possible to see through the entire channel while still clearly visualizing the flow near the ultrahydrophobic surfaces. The emission from the tracer particles was collected by a high-speed digital camera (Phantom 4.1) at frame rates from 100 to 400 frames/s. As with standard PIV techniques, successive images were captured with a given delay time, and the flow velocities were calculated by correlating particle displacement using a commercial PIV software package (DAVIS, LaVision). In order to capture the velocity profile above the oblique microridges, a 60× objective was used to obtain a 187×187 μm^2 view range, so that μPIV measurements could be made using the same microchannels used in the confocal microscopy measurements.

D. Computational fluid dynamics analysis

A series of numerical simulations were performed using FLUENT to both confirm and extend the experimental mixing measurements. The dimensions of the rectangular microchannel were set at 100 μm wide, 50 μm high, and 20 mm long, in order to match the experimental flow cell described above. The geometry was discretized with a uniformly dense, three-dimensional, structured mesh containing 1.75×10^6 nodes created from equisized hexahedral volumes. The inlet was divided into two species having the properties of water, with a diffusion coefficient set to match the diffusion coefficient of the fluorescent dye used in the microchannel mixing experiments. A mass flux boundary condition was set at the inlet and exit, matching the experimentally imposed conditions. The no-slip boundary condition was used for all the solid bounding walls, while the air-water interface supported by the microridges was assumed to be shear-free and flat. At the flow rates and pressure drops probed in our experiments, we have shown that the assumption of no deflection of the free surface is reasonable [23,24].

The simulations were all found to converge within 3000–3500 iterations, and the results were found to be insensitive to further mesh refinement. Given that a regularly structured hexahedral mesh was used in the numerical simulation, the degree of mixing along the flow direction was quantified by calculating the spatially weighted standard deviation of the species concentration at each node point for a series of evenly spaced slices in the yz plane along the length of the flow channel,

$$\sigma = \sqrt{\langle (c - \langle c \rangle)^2 \rangle}. \quad (1)$$

Here the angular brackets denote a spatial average over all node values in the plane being analyzed, and c represents the concentration of the fluorescent dye. With the grid density properly set, each standard deviation value takes into account nearly 1000 samples per plane of examination. In order to quantify the mixing, a dimensionless degree of mixing was calculated,

$$\Phi = \left(\frac{0.5 - \sigma}{0.5} \right). \quad (2)$$

The degree of mixing varies from $\Phi = 0$, when the system is completely unmixed, to a value of $\Phi = 1$, when the flow is completely mixed. The same general procedure was used to quantify the degree of mixing for the experimental measurements, using the standard deviation of the normalized fluorescence intensity.

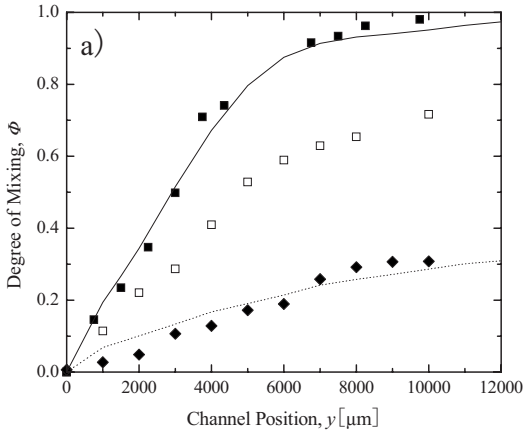

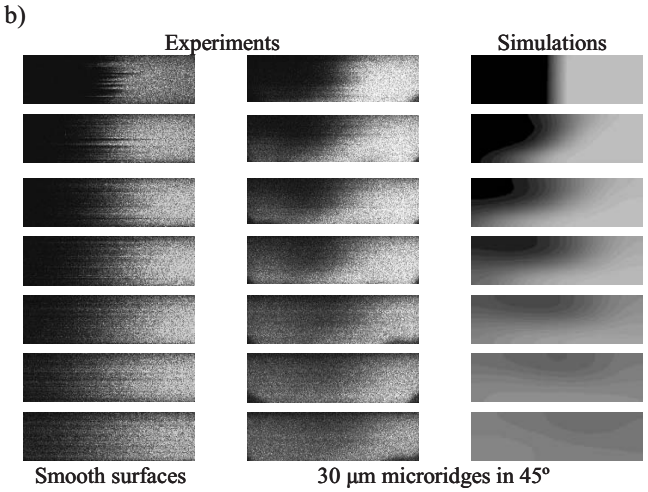

FIG. 2. (a) Comparison between microchannels with ultrahydrophobic surface with 30 μm hydrophobic microridges (■) and hydrophilic microridges (□) at 30 μm spacing at 45° and smooth surface (◆). Simulations of smooth surface (·····) and 30 μm microridges at 30 μm spacing at 45° (—) are also shown. (b) Flow patterns of the channel's intersections from the inlet along the flow direction with 750 μm spacing.

To validate our numerical simulations, the flow through a rectangular microchannel with smooth no-slip walls was first simulated. The velocity profiles and pressure drops were found to quantitatively agree with the closed-form analytical solution for low Reynolds number flow through a rectangular channel.

III. RESULTS AND DISCUSSION

Using the techniques described above in Sec. II A, a series of ultrahydrophobic surfaces were fabricated in order to quantify the effects of microridge geometry and Péclet number on the mixing length. In Fig. 2, the secondary flow patterns and degree of mixing are presented for the flow at

Pe=435 past an ultrahydrophobic surface with $w=30$ μm wide microridges spaced $d=30$ μm apart and aligned at a $\theta=45°$ angle to the flow direction. To quantify the mixing enhancement, the flow patterns and degree of mixing for flow down an identical microchannel with smooth walls are used as a baseline for comparison, and are presented alongside the ultrahydrophobic surface data in Fig. 2. In Fig. 2(a), the degree of mixing Φ is plotted as a function of position down the microchannel in the z direction. Close to the inlet, the degree of mixing increase with position along the channel, and eventually asymptotically approaches complete mixing, $\Phi=1$. For the ultrahydrophobic geometry presented in Fig. 2(a), 95% mixing is achieved after approximately $L_{95\%}\approx 8$ mm.

As seen in the experiments and the simulations in Fig. 2(b), for the flow over a smooth channel, the interface between the dyed and undyed fluid is not distorted, but does begin to soften along the length of the channel as diffusion of the fluorescent dye begins to mix the two species. The mixing length in this case can be approximated by

$$L_{mix} \approx U(W^2/D) = W\,\mathrm{Pe} \tag{3}$$

where $W=100$ μm is the width of the channel, $U=1$ cm/s is the average velocity in the channel, and $D=2.3\times 10^{-5}$ cm^2/s is the self-diffusion coefficient of the fluorescent dye in water at 25 °C [36]. The diffusion time for a particle to migrate from one side of the channel to another is approximately $t_D=w^2/D\approx 4.4$ s. For the smooth microchannel in these experiments and simulations, the diffusive mixing length required is approximately $L_{95\%}\approx 4.4$ cm, which is longer than the length of the microchannel. Using this estimate, the results for the ultrahydrophobic surface correspond to a sixfold mixing enhancement.

For comparison, a hydrophilic mixing channel with the same surface structure as the ultrahydrophobic surface was fabricated and tested. The results for the hydrophilic channel are presented alongside those for the ultrahydrophobic surfaces in Fig. 2(a). For the case of the hydrophilic microridges, confocal microscopy clearly shows that the water intrudes into the gaps between the microridges, displacing the air present in the hydrophobic case, and eliminating the shear-free air-water interface. The presence of the air-water interface between adjacent hydrophobic microridges can be imaged using confocal microscopy, and its deflection as a function of pressure has been quantitatively measured in the past using laser confocal metrology [23]. The hydrophilic surfaces and the resulting mixing enhancement are similar to those tested in the recent literature [2,29]. Our measurements demonstrate the presence of a helical secondary flow for both the hydrophilic and hydrophilic microridges, although the secondary flow is found to be significantly stronger for the ultrahydrophobic case. From the data in Fig. 2(a), it is clear that the presence of both hydrophobic and hydrophilic microridges enhances mixing well beyond the smooth surface limit. The presence of the shear-free air-water interface along the ultrahydrophobic surface increases the mixing efficiently by a factor of approximately 2 over the hydrophilic microridges.

As seen by the confocal images in Fig. 2(b), the improved mixing is achieved in large part through the generation of a helical secondary flow that folds and stretches the fluid elements, thereby reducing the average distance the fluorescent dye must diffuse. The presence of slip along the shear-free air-water interface reduces the resistance to flow in the direction of the microridges, and partially deflects the flow near the ultrahydrophobic surface. This can be observed in the experiments and the numerical simulations in Fig. 2(b). Near the bottom wall, the dyed water on the right side of the microchannel is observed to move to the left. Conservation of mass dictates that the undyed water on the left side of the microchannel is forced up the left wall, and then to the right along the top surface of the microchannel, resulting in the secondary helical flow observed within the rectangular microchannel.

The strength of the helical flow can be more precisely quantified through the flow deflection angle, or, equivalently, the distance required for the fluid to make one complete revolution around the rectangular microchannel. For the ultrahydrophobic surface used in Fig. 2, it takes approximately 15 mm for the fluid to complete one revolution around the microchannel. This is equivalent to a $\Omega=2.0°$ deflection angle. By contrast, the deflection angle for the hydrophilic microridges was found to be only $\Omega=1.4°$. The correlation between the flow patterns measured experimentally and the patterns predicted by the numerical simulation is very good. This, however, is not surprising, considering the quantitative agreement between the numerical simulation prediction for the degree of mixing and the experimental data in Fig. 2(a). The agreement between the experiments and simulation in both the flow pattern and the degree of mixing suggests that the numerical simulation is capturing the necessary physics to be used both as a design tool to optimize the geometry of the ultrahydrophobic surface for mixing and as a detailed probe of the flow kinematics responsible for the enhanced mixing.

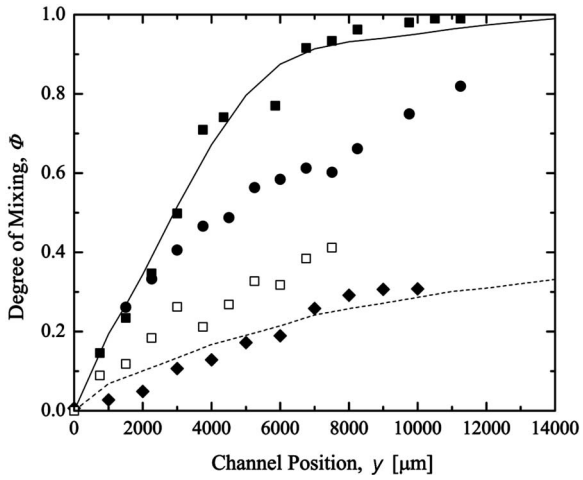

FIG. 3. Comparison between microchannels with ultrahydrophobic surface with 30 μm microridges at 30 μm spacing at 45° under Péclet numbers of 435 (■), 2175 (●), and 4350 (□). Smooth surface with Pe=435 (♦) and simulations of smooth surface (·····) and 30 μm microridges at 30 μm spacing at 45° (—) are also shown.

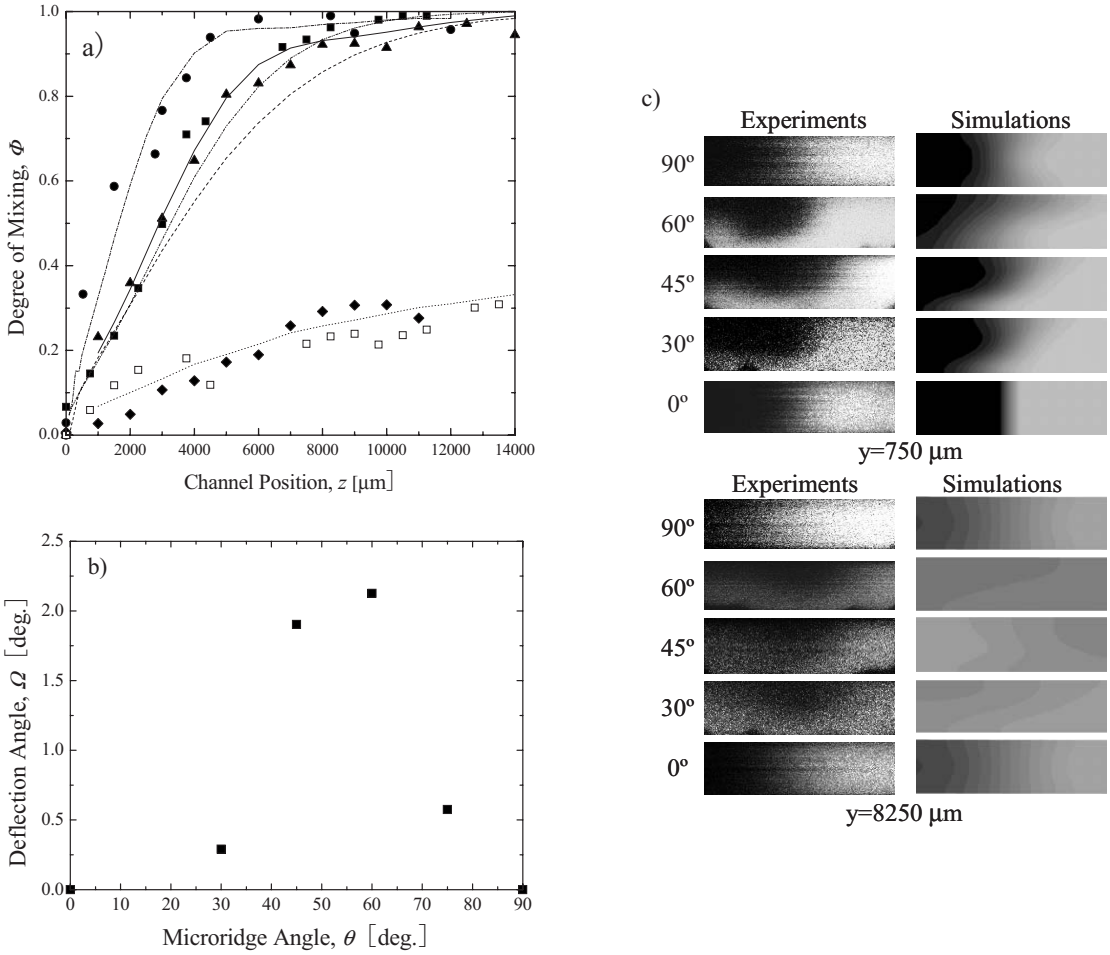

FIG. 4. (a) Degree of mixing of ultrahydrophobic surfaces with 30 μm microridges at 30 μm spacing and 30° (▲), 45° (■), 60° (●), and 90° (□) to the flow direction. Smooth surface (◆) is also shown. Experimental data are compared with numerical simulation of smooth surface (·····) and 30 μm microridges at 30 μm spacing and 30° (-···-), 45° (—), 60° (--), and 75° (- -) to the flow direction. (b) Flow patterns of the channel intersections in different channel positions 750 and 8250 μm away from the inlet.

The effect of changing the Péclet number on the mixing enhancement achieved for flows through a microchannel having the same ultrahydrophobic surface discussed above is presented in Fig. 3. To achieve higher Péclet numbers, the volume flow rate through the microchannel was increased by factors of five and ten times the original flow rate. It should be noted that, for this ultrahydrophobic surface design, significantly higher Péclet numbers were not achievable, because the pressure within the microchannel would become large enough to drive the air-water interface into the gap between the microridges [23,24], and we expect that the results would then approach the case of the hydrophilic, fully wetted grooves presented in Fig. 2. As expected, as the Péclet number is increased, and the relative importance of the diffusion to convection is decreased, the fluids mix more slowly. Increasing the Péclet number is found to have no effect on the strength of the secondary helical flow; the deflection angle was found to be insensitive to increasing the flow strength.

If the flow were chaotic, it has been shown that the stretching and folding of the fluid volume reduces the distance over which diffusion must act exponentially with increasing distance down the channel, $\Delta L \propto \exp(-y/\lambda)$ [37]. Here λ is the characteristic length determined by the chaotic flow. It can be shown that this results in logarithmic dependence of the mixing length with Péclet number, $\Delta y_{\mathrm{mix}} \sim \lambda \ln(\mathrm{Pe})$ [2,29]. Plotting mixing length from Fig. 3 versus Péclet number, we do not find a logarithmic dependence, but a power law dependence much closer to $\Delta y_{\mathrm{mix}} \sim \mathrm{Pe}^{1/2}$. This suggests that our flow is not chaotic; however, it would be straightforward to design a more complex surface pattern, which would result in a chaotic flow and further increase the mixing enhancement achieved using these simple angled microridges.

A series of experiments and numerical simulations were performed to try to optimize the mixing enhancement achieved through the use of ultrahydrophobic surfaces. In Fig. 4, the effect of the angle of the hydrophobic microridges was investigated by varying the angle of the microridges in the range $30° \leq \theta \leq 90°$. The mixing channel's geometry was fixed at 50 μm high and 100 μm wide, while the size and spacing of the microridges were held fixed at $d=30$ μm and $w=30$ μm, respectively, and the Péclet number fixed at Pe=435. The degree of mixing of different angle microridges

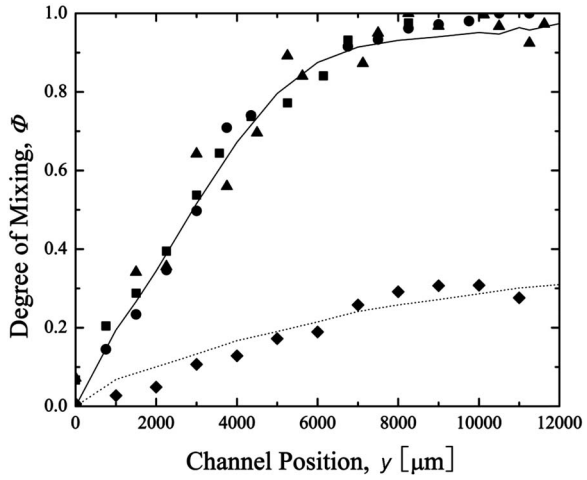

FIG. 5. Degree of mixing of ultrahydrophobic surface with 30 μm microridge (■), 60 μm microridge (●), and 90 μm microridge (▲) at 30 μm spacing and 45° to the flow direction, compared with smooth surface (◆), and numerical simulation of 30 μm microridge at 30 μm spacing and 45° (—) and smooth surface (·····).

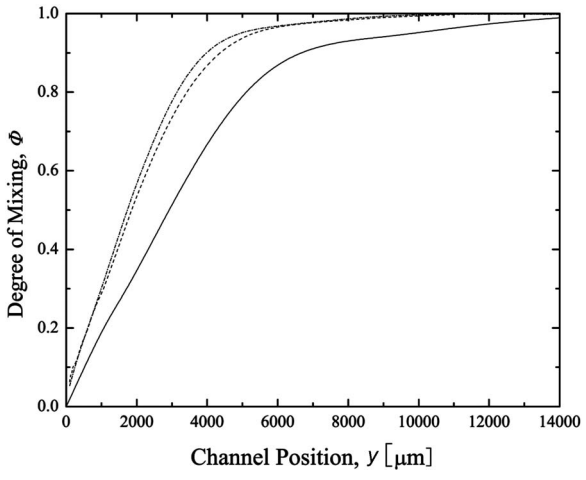

FIG. 6. Numerical simulation of 30 μm microridges at 30 (—), 60 (- -), and 90 μm (-·-) spacing with 45° angle.

is shown in Fig. 4(a). For each case examined, with the exception of the θ=90° case, where the microridges are aligned normal to the flow direction, the presence of the shear-free band generated a helical flow, which in turn significantly decreased the mixing time. However, the relationship between angle of attack and mixing length is not a monotonic function. By increasing the angle from θ=0° to 60°, the required mixing length decreases quite rapidly; however, as the angle of the microridges is increased further from θ=60° to 90°, the mixing length is found to increase back to the smooth surface diffusive mixing limit. Overlaid upon the experimental data are the predictions of the numerical simulations for the same flow geometries and flow conditions. The excellent agreement between the simulation and the experiments gives us the confidence in the numerical simulations to move forward and use the numerical simulations as a tool for extending the experimental observations to different flow geometries. Also included in Fig. 4(a) are the results from the numerical simulation of the flow past an ultrahydrophobic surface with microridges aligned at a θ=75° to the flow direction. The mixing length for the θ=75° case is significantly longer than in the θ=60° case. These simulations suggest that, for the ultrahydrophobic surfaces tested here, θ=60° is close to the optimal microridge angle for enhanced mixing, although further simulations or experiments need to be performed to more precisely determine the optimal ultrahydrophobic surface geometry. The deflection angles of the secondary helical flow generated by the series of microridges in different angles are compared in Fig. 4(b). This is illustrated by the increase in the deflection angle. Improvement to the mixing is found to correlate directly with the strength of the secondary flow and with increasing microridge angle up to a maximum θ=60°, as demonstrated in Fig. 4(b).

The secondary flow structure induced by the presence of the shear-free air-water interface supported by the hydrophobic microridges is presented in Fig. 4(c) as a series of confocal microscopy images. As indicated by our measurements of deflection angle, by increasing the angle of the microridges up to θ=60°, the fluid is observed to rotate more quickly, resulting in the production of more interfacial area between the fluorescently tagged and untagged fluids, and reducing the distance needed to diffuse. This observation is in contrast to the analytical solution for the flow over periodic wetted grooves aligned at an oblique angle to the flow direction, where the maximum helical flow strength was observed at 45° [26,29]. As seen from the images in Fig. 4(c), at the Péclet number Pe=435, in these experiments diffusion occurs relatively quickly, softening the interface between the fluorescently tagged and untagged fluids, and effectively mixing the fluids after only a small number of rotations around the microchannel. The flow patterns at 90° angle are also shown in Fig. 4(c). As expected, no significant difference is discernible between the smooth surface and the hydrophobic microridges aligned in the flow direction. In addition, the agreement between the flow structures observed in the experiments and predicted by the numerical simulations is quite good at positions near both the entrance and exit of the microchannel.

A series of experiments was designed to investigate the role of microridge size and spacing on mixing. Ultrahydrophobic surfaces with d=30, 60, and 90 μm wide microridges spaced w=30 μm apart and at a θ=45° angle to the flow direction were fabricated. The degree of mixing of each is shown in Fig. 5 for a flow at a Péclet number of Pe=435, and compared with the mixing achieved along a smooth surface and the predictions of numerical simulations. In contrast to the large effect on the mixing length of the angle of the microridge, the mixing length was found to be relatively insensitive to the size of the microridges over the range of size tested in our experiments; saturation was achieved very quickly with d=90 μm wide microridges, and no improvement in mixing was observed with further decreases to the microridge size or increases to the percentage of the shear-free interface.

A series of numerical simulations were run to determine if the mixing enhancement is significantly affected by increas-

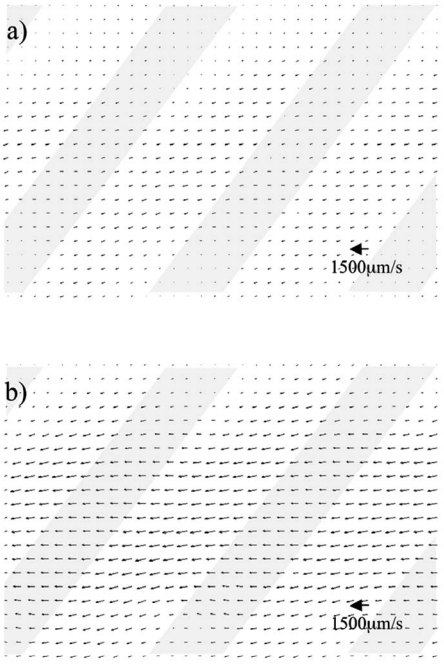

FIG. 7. Velocity profile of the μ PIV measurement (a) along the ultrahydrophobic surface with $d=30$ μm wide microridges spaced $w=30$ μm apart at a $\theta=45°$ angle to the flow direction and at a Péclet number of Pe=217 and (b) 10 μm above the same ultrahydrophobic surface.

ing the size of the shear-free air-water interface between microridges. In the simulation, the microridge size was held fixed at $d=30$ μm and the microridge spacing was increased from $w=30$ to 60, and finally to 90 μm. As seen in Fig. 6(a), increasing the amount of shear-free interface does increase the mixing rate; however, the effect is observed to saturate beyond a microridge spacing of approximately $w>60$ μm. Thus, it is clear that the mixing enhancement effect achieved in microchannels with ultrahydrophobic surfaces is less sensitive to the amount of shear-free air-water interface than it is to the angle that the microridges make with the flow direction.

In order to further probe the flow kinematics near the ultrahydrophobic surface, a series of μPIV measurements were made of the flow past an ultrahydrophobic surface with ridges spaced 30 μm apart and aligned at a 45° to the flow at a Péclet number of Pe=217. In Fig. 7, 2D μPIV velocity profiles are presented for xy planes just above the ultrahydrophobic surface and 10 μm above the ultrahydrophobic surface in Figs. 7(a) and 7(b), respectively. The position of the microridges is superimposed over both data sets. Just above the ultrahydrophobic surface, as expected, the water above the microridges is not flowing, following the no-slip boundary condition, while the fluid above the shear-free air water interface is found to demonstrate a considerable slip velocity on the order of up to 40.5% the average velocity in the microchannel and a maximum angle of up to 8.3° from the flow direction. This result is consistent with the results of Ou and Rothstein [24]; however, the slip velocity is not tangent to the flow direction, but is instead aligned at a slight angle to the flow direction. As the image plane is moved

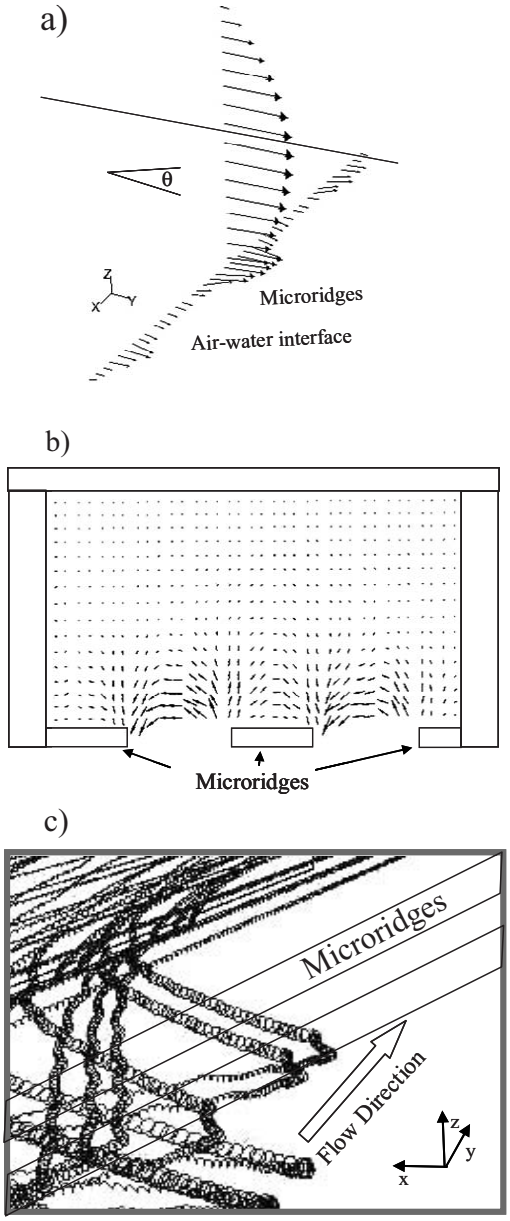

FIG. 8. Series of flow profiles generated by numerical simulation of flow past microchannel with $d=30$ μm wide microridges spaced $w=30$ μm apart at a $\theta=45°$ angle to the flow direction and at a Péclet number of Pe=435. (a) Complete velocity profile near the shear-free air-water interface, (b) the xz component of the velocity profile of the cross section of the channel, and (c) streak lines highlighting the three-dimensionality of the flow near the ultrahydrophobic surface.

10 μm away from the ultrahydrophobic surface in Fig. 7(b), the presence of the ultrahydrophobic surface is still observed. What is interesting is that above the shear-free air-water interface the fluid is still moving at a modest angle to the flow direction, although the angle appears to be reduced when compared to Fig. 7(a); however, the flow above the no-slip microridge is aligned with the flow direction.

The predictions of the numerical simulations match the μPIV results very well; however, unlike μPIV, which is limited to measurements of the x and y components of the fluid

velocity, the numerical simulations can be used to further investigate the three-dimensionality of the flow. As seen in Fig. 8, the velocity along the air-water interface shows not only an x component of velocity that drives the helical flow, but also a z component, which indicates a vertical movement of the fluid as the fluid decelerates upon transitioning from the shear-free interface to the no-slip microridge, and vice versa. The result is a more tortuous path for the fluid flowing near the ultrahydrophobic surface, and an additional mechanism beyond the full-channel helical flow for enhancing mixing. This is demonstrated by the streak lines shown in Fig. 8(c), which exhibit a small radius of rotation near the ultrahydrophobic surface. This mixing mechanism suggests that, if fluorescently tagged and untagged fluids could be stacked vertically rather than horizontally, enhanced mixing could be observed even in the $\theta=90°$ case. Additionally, our previous research with ultrahydrophobic surfaces showed that drag reduction was maximized with decreasing channel height, and that the influence of the shear-free interface was observed roughly one microridge width into the channel [24]. This suggests that, if the height of the mixing microchannel is decreased close to the dimension of the microridge spacing, these rotations induced by the "tripping" of the fluid may dramatically improve the efficiency of mixing produced by the global helical flow, resulting in a fully chaotic flow.

IV. CONCLUSIONS

The mixing effect of the ultrahydrophobic surfaces was studied in this paper with a series of experiments, and simulated with full size numerical models. The ultrahydrophobic surfaces with a series of pattern designs were fabricated with soft lithography techniques and assembled into micromixing channels. The correlation between the effect of mixing and the pattern designs, such as the angle and size of the microridges, was studied. Fluorescently tagged and untagged deionized water was fed into the microchannel, and the flow behaviors were imaged using confocal microscopy. A series of full-scale numerical models were built via commercial simulation software package, and the experimental results were directly compared with the simulations. Significant mixing enhancement was achieved by using ultrahydrophobic surfaces with diagonal microridges. The mixing length was reduced as much as ten times when compared to a smooth hydrophobic surface. Enhanced mixing was achieved by stretching and folding the interface between the two species through a helical secondary flow generated by the unique geometry and periodic slip of no-slip interface engineered by using ultrahydrophobic surfaces. The slip velocity induced along a shear-free air-water interface aligned obliquely to the flow direction is the driving force for the secondary helical flow and the enhanced mixing. The effect of mixing was maximized by changing the geometry of the surface structure to produce the most favorable slip velocity. For 30 μm microridges with 30 μm spacing and 60° angle to the flow direction showed the best mixing performance in the experiments. The mixing behavior is less sensitive to the area ratio of the shear-free air-water interface than to the angle of the microridges. Both the flow behavior and the degree of mixing measured within our experiments were quantitatively matched by our numerical simulation. The results suggest that further optimization of the surface structure geometry through the generation of chaotic flow patterns can be designed in future numerical simulations.

ACKNOWLEDGMENTS

The authors would like to thank Thomas McCarthy and John Nicholson of the University of Massachusetts for their assistance in fabricating the ultrahydrophobic surfaces. The authors would also like to thank 3M for financial support and the office of Naval Research under Grant N00014-06-1-0497 for partial support of this research.

[1] X. Niu and Y.-k. Lee, J. Micromech. Microeng. **13**, 454 (2003).
[2] A. D. Stroock, S. K. W. Dertinger, A. Ajdari, I. Mezic, H. A. Stone, and G. M. Whitesides, Science **295**, 647 (2002).
[3] N. Schwesinger, T. Frank, and H. Wurmus, J. Micromech. Microeng. **6**, 99 (1996).
[4] F. B. Knight, *Essentials of Brownian Motion and Diffusion* (American Mathematical Society, Providence, RI, 1981).
[5] R. H. Liu, M. A. Stremler, K. V. Sharp, M. G. Olsen, J. G. Santiago, R. J. Adrian, H. Aref, and D. J. Beebe, J. Microelectromech. Syst. **9**, 190 (2000).
[6] R. F. Ismagilov, A. D. Strook, P. J. A. Kenis, G. Whitesides, and H. A. Stone, Appl. Phys. Lett. **76**, 2376 (2000).
[7] A. E. Kamholz, B. H. Weigl, B. A. Finlayson, and P. Yager, Anal. Chem. **71**, 5340 (1999).
[8] M. A. Burns, B. N. Johnson, S. N. Brahmasandra, K. Handique, J. R. Webster, M. Krishnan, T. S. Sammarco, P. M. Man, D. Jones, D. Heldsinger, C. H. Mastrangelo, and D. T. Burke, Science **282**, 484 (1998).
[9] J. Happel and H. Brenner, *Low Reynolds Number Hydrodynamics* (Prentice-Hall, Englewood Cliffs, NJ, 1965).
[10] D. Gobby, P. Angeli, and A. Gavriilidis, J. Micromech. Microeng. **11**, 126 (2001).
[11] F. G. Bessoth, A. J. deMello, and A. Manz, Anal. Commun. **36**, 213 (1999).
[12] R. Chella and J. M. Ottino, Ind. Eng. Chem. Fundam. **24**, 170 (1985).
[13] W. Barthlott and C. Neinhuis, Planta **202**, 1 (1997).
[14] D. Oner and T. J. McCarthy, Langmuir **16**, 7777 (2000).
[15] J. Bico, C. Marzolin, and D. Quere, Europhys. Lett. **47**, 220 (1999).
[16] J. P. Youngblood and T. J. McCarthy, Macromolecules **32**, 6800 (1999).
[17] A. Y. Fadeev and T. J. McCarthy, Langmuir **15**, 3759 (1999).
[18] W. Chen, A. Y. Fadeev, M. C. Hsieh, D. Oner, J. P. Youngblood, and T. J. McCarthy, Langmuir **15**, 3395 (1999).

[19] Z. Yoshimitsu, A. Nakajima, T. Watanabe, and K. Hashimoto, Langmuir **18**, 5818 (2002).
[20] R. N. Wenzel, Ind. Eng. Chem. **28**, 988 (1936).
[21] A. B. D. Cassie and S. Baxter, Trans. Faraday Soc. **40**, 546 (1944).
[22] J. Kim and C.-J. Kim, in *Proceeding of the IEEE International Conference on Micro Electro Mechanical Systems (MEMS)* (IEEE, Las Vegas. NV, 2002), p. 479.
[23] J. Ou, B. Perot, and J. P. Rothstein, Phys. Fluids **16**, 4635 (2004).
[24] J. Ou and J. P. Rothstein, Phys. Fluids **17**, 103606 (2005).
[25] P. Joseph, C. Cottin-Bizonne, J. M. Benoit, C. Ybert, C. Journet, P. Tabeling, and L. Bocquet, Phys. Rev. Lett. **97**, 156104 (2006).
[26] A. Ajdari, Phys. Rev. E **65**, 016301 (2002).
[27] A. A. Darhuber, J. P. Valentino, J. M. Davis, and S. M. Troian, Appl. Phys. Lett. **82**, 657 (2003).
[28] A. A. Darhuber, J. Z. Chen, J. M. Davis, and S. M. Troian, Philos. Trans. R. Soc. London **362**, 1037 (2004).
[29] A. D. Stroock, S. K. Dertinger, G. M. Whitesides, and A. Ajdari, Anal. Chem. **74**, 5306 (2002).
[30] Y.-K. Lee, J. Deval, P. Tabeling, and C.-M. Ho, in *Proceedings of the IEEE International Conference on Micro Electro Mechanical System (MEMS)* (IEEE, Interlaken, Switzerland, 2001), p. 483.
[31] C. Simonnet and A. Groisman, Phys. Rev. Lett. **94**, 134501 (2005).
[32] T. J. Johnson, D. Ross, and L. E. Locascio, Anal. Chem. **74**, 45 (2002).
[33] B. Zhao, J. S. Moore, and D. J. Beebe, Science **291**, 1023 (2001).
[34] J. A. Pathak, D. Ross, and K. B. Migler, Phys. Fluids **16**, 4028 (2004).
[35] T. Burghelea, E. Segre, I. Bar-Joseph, A. Groisman, and V. Steinberg, Phys. Rev. E **69**, 066305 (2004).
[36] M. Holz, S. R. Heil, and A. Sacco, Phys. Chem. Chem. Phys. **2**, 4740 (2000).
[37] J. M. Ottino, *The Kinematics of Mixing: Stretching, Chaos, and Transport* (Cambridge University Press, Cambridge, U.K., 1989).